Structural Study on the Micelle Formation of Poly(ethylene oxide)–Poly(propylene oxide)–Poly(ethylene oxide) Triblock Copolymer in Aqueous Solution

Kell Mortensen* and Jan Skov Pedersen

Department of Solid State Physics, Risø National Laboratory, DK-4000 Roskilde, Denmark

Received July 9, 1992; Revised Manuscript Received October 30, 1992

ABSTRACT: The phase behavior of poly(ethylene oxide)–poly(propylene oxide)–poly(ethylene oxide) (PEO–PPO–PEO) triblock copolymers dissolved in water has been studied using small-angle neutron scattering. The structural properties have been studied as a function of polymer concentration and temperature. At low temperature ($T \leq 15$ °C) and low polymer concentrations the unimers are fully dissolved Gaussian chains with radius $R_g = 17$ Å. Close to ambient temperature, the hydrophobic nature of PPO causes aggregation of the polymers into spherical micelles with core sizes of the order of 40–50 Å, somewhat temperature dependent. The concentration of micelles increases roughly linearly with temperature, until either a saturation is reached, where all polymers are part of a micelle, or the volume density of micelles is so high that they lock into a crystalline structure of hard spheres. In the 60–70 °C temperature range, the micellar structure changes from spherical form to prolate ellipsoid, leading to a decreasing intermicelle interaction. At high concentration, this causes melting of the cubic lattice and leads successively to the formation of a rodlike structure with hexagonal symmetry. Close to 95 °C, large aggregates of polymers ordered in lamellae structure are formed, leading to an opaque suspension.

I. Introduction

Aqueous solutions of poly(propylene oxide) (PPO) exhibit dramatic temperature dependence. Below approximately 15 °C, water is a good solvent for PPO, whereas PPO at higher temperatures aggregates. Poly(ethylene oxide) (PEO), on the other hand, is dominantly hydrophilic within the temperature range from 0 to 100 °C. With blocks of PEO and blocks of PPO combined into single polymer chains, one can therefore expect amphiphilic characteristics with interesting aggregation phenomena.

A number of studies have been made in the attempt to describe such aggregates of PEO–PPO–PEO block copolymers in water, however with considerable confusion concerning the association properties. Using ultrasonic velocity and light scattering studies, however, Rassing and Attwood provided in 1983 a clear indication of micelle formation.[1] Further evidence of micelles was given by the dynamic light scattering studies of Zhou and Chu in 1987.[2,3] Since then, the micelle formation of PEO–PPO–PEO systems has been confirmed based on both dynamic light scattering studies[4,5] and neutron scattering techniques.[4,6,7]

At temperatures close to ambient it is well known that high-concentration polymer solutions exhibit a dramatic change in viscosity, revealing a "thermoreversible gelation".[4,5,9,10] Several mechanisms have been proposed as driving forces for this thermal gelation. Rassing and Attwood related the gel transition to intrinsic changes in the micellar properties.[1] Vadnere et al. discussed the gelation in terms of entropic changes, involving locally ordered water molecules close to the hydrophobic units,[9] whereas Wanka et al.[4] and Wang and Johnston[10] in addition speculated at the possibility of an ordered three-dimensional structured state or network. Recently, structural neutron scattering studies unambiguously showed that the observed change in viscosity is due to a "hard-sphere crystallization" as the micelle concentration approaches the critical volume fraction of 0.53.[6-8]

In the present paper we report structural properties of aqueous solutions of $EO_{25}PO_{40}EO_{25}$, with special reference to low polymer concentrations. The study is based on small-angle neutron scattering experiments. It is shown that micelles are formed whenever a phase line of critical micellation concentration (c_{cm}) and critical micellation temperature (T_{cm1}) is crossed. The micelles are to a good approximation spherical objects composed of a central core of dense poly(propylene oxide) and with an outer corona of hydrated poly(ethylene oxide) units. The intermicellar interactions are, in spite of the flexible PEO blocks dispersed in the water, basically as for hard spheres, and one even observes a hard-sphere crystallization as mentioned above. Above approximately 70 °C the spherical micellar structure of the aggregates changes into prolate ellipsoidal aggregates.

II. Experimental Section

A. Sample. The triblock copolymer $EO_{25}PO_{40}EO_{25}$, abbreviated P85, was obtained from Serva AG, Heidelberg, Germany, and used without further purification. It has a declared molecular mass of 4.5 kDa, 1100 Da for each of the PEO blocks and 2320 Da for PPO. $EO_{25}PO_{40}EO_{25}$ was dissolved in water at 5 °C, forming a transparent, homogeneous polymer solution. Deuterated water (D_2O) was used to get good contrast and low background for the neutron scattering experiments.

The samples were mounted in sealed quartz containers (Suprasil from Hellma, Germany) with a 2-mm flight path. The neutron beam at the sample position was 7 mm in diameter. For the neutron spectra of water, used for calibration, a 1-mm-thick quartz container was used.

B. SANS. Small-angle neutron scattering experiments were performed using the Risø SANS facility, which is a flexible instrument covering scattering vectors ($|\mathbf{q}| = q = (4\pi/\lambda)\sin(\theta/2)$) from 0.002 to 0.5 Å^{-1} with variable neutron wavelength resolution ($\Delta\lambda/\lambda$). (In the expression for the scattering vector q, θ is the scattering angle and λ is the neutron wavelength. $\Delta\lambda$ is the full-width at half-maximum value of the neutron flux versus wavelength distribution.) The results shown below were obtained using 15-, 6-, and 3-Å neutrons, with sample-to-detector distances of respectively 6, 3, and 1 m, giving scattering vectors q in the ranges 0.002–0.02, 0.01–0.1, and 0.05–0.5 Å^{-1}, respectively. The neutron wavelength resolution used was $\Delta\lambda/\lambda = 0.18$, and the neutron beam collimation was determined by the pinhole sizes of 16- and 7-mm diameter at the source and sample positions, respectively, and collimation lengths of 6, 3, and 1 m, respectively, for the three settings. The smearing induced by the different instrumental setups is included in the data analysis discussed below.[11]

The scattering data were corrected for background arising from the quartz container with D_2O and from other sources, as

0024-9297/93/2226-0805$04.00/0

measured with the neutron beam blocked by plastic containing boron at the sample position. The incoherent scattering from H_2O was used to take deviation from a uniform detector response into account.

The scattering patterns discussed in the present paper are all azimuthal isotropic. The data have therefore been reduced to the one-dimensional $I(q)$ scattering functions only dependent on the absolute value of q.

The $I(q)$ scattering function was Fourier-transformed using the indirect method of Glatter,[12] giving the distance distribution function $p(R)$, which is the scattering density correlation function multiplied by the distance squared. In the method of Glatter, one uses the form $p(R) = \sum a_n B_n(R)$, where B_n are cubic-spline functions and a_n are parameters to be determined by a constrained least squares analysis. In addition, an independent uniform background describing the incoherent scattering has been included in the data analysis.[13] The error bars on $p(R)$ as determined by this Fourier transformation technique and as shown in the figures discussed below have by simulation studies been found to be overestimated by a factor of the order of 2–3.[14]

III. Results and Discussion

In Figure 1 are shown characteristic scattering functions as represented by the 4, 12, and 25 wt % aqueous solutions of P85 obtained in the temperature range 5–80 °C. (More detailed scattering data, including a larger q range and error bars will be shown below.) From these scattering curves dramatic temperature dependencies appear: at low temperature, the scattering functions all show relatively weak q dependence and only small intensities. At higher temperatures the intensity increases, reflecting association of molecules into larger aggregates. In an intermediate temperature range, the scattering function for the more concentrated solutions ($c \geq 1$ wt %) is dominated by a pronounced correlation peak, and for polymer concentrations above approximately 20 wt %, a sudden change in the peak line width is seen (cf. Figure 1c). At even higher temperatures, however, this correlation peak changes in characteristics and disappears for the lowest concentrations, while the low-angle scattering intensity shows a marked increase (cf. Figure 1a). In the following, we will separately discuss the three regimes: (i) low-temperature, low-concentration dissolved polymers, (ii) ambient-temperature micellar liquid, and (iii) high-temperature properties. Moreover, we will discuss the intermicellar interactions as determined from the interference effects observed in the scattering function.

A. Gaussian Unimers. At low temperature both poly(propylene oxide) and poly(ethylene oxide) are hydrophilic. The block copolymers therefore appear as independent, fully dissolved polymer chains. In Figure 2a is shown the scattering function of a 4 wt % polymer solution as obtained by the three experimental settings discussed above. Figure 2b shows the distance distribution function $p(R)$ as obtained from indirect Fourier transformation of $I(q)$. The long tail at large R values is characteristic for an open structure. The scattering function is accordingly in good agreement with that of a randomly distributed coil, following the Debye function

$$I(q) = M_p N_A c \Delta b^2 x^{-2}(1 + x + e^x) + I_{inc} \qquad (1)$$

where $x = (qR_g)^2$, R_g being the polymer radius of gyration. $M_p = 4500$ is the molecular mass, N_A is Avogadro's number, c is the polymer concentration, and $\Delta b = \Sigma b - \rho_w V_P/M_p$ is the contrast factor, where $\Sigma b = 33.9 \times 10^{-12}$ cm is the coherent scattering length of the polymer, ρ_w is the scattering length density of water (D_2O), and $V_P = 7436$ Å^3, the volume of the dry polymer. (With the scattering length density of PEO equal to 0.572×10^{-14} cm/Å^3, that of PPO equal to 0.347×10^{-14} cm/Å^3, and that of D_2O equal to 6.36×10^{-14} cm/Å^3, the scattering contrast between PEO and PPO is negligible relative to the scattering contrast between the polymer and solvent.) I_{inc} is the incoherent background. The scattering function gives the radius of gyration, $R_g = 17$ Å. For comparison, the hydrodynamic radius obtained from dynamic light scattering is $R_h = 18$ Å.[5]

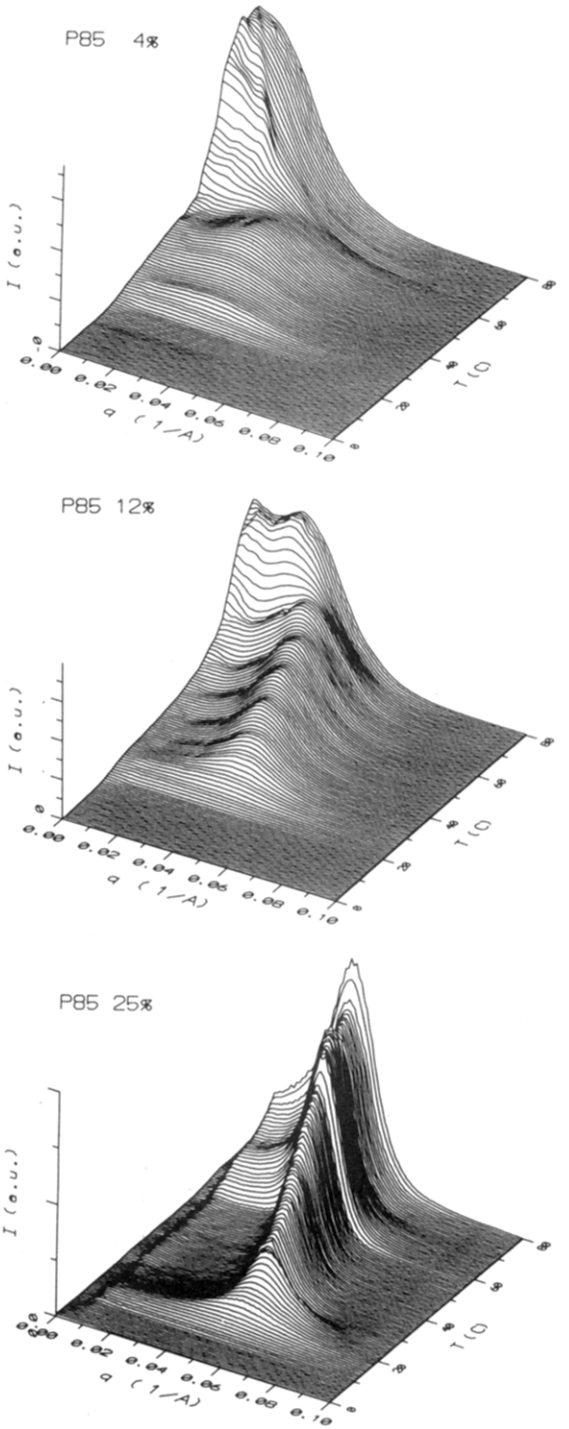

Figure 1. Scattering function I vs q of aqueous solutions of $EO_{25}PO_{40}EO_{25}$ as obtained in the 0–80 °C temperature range: (a) 4, (b) 12, and (c) 25 wt % polymer concentrations. (The apparent oscillations with temperature in (b) is an artifact of the plotting routine.)

B. Micelle Formation. At temperatures close to ambient the poly(propylene oxide) part of the polymer chain is no longer soluble in water. The resulting amphiphilic character of $EO_mPO_nEO_m$ triblock copolymers leads to formation of various aggregates, depending on

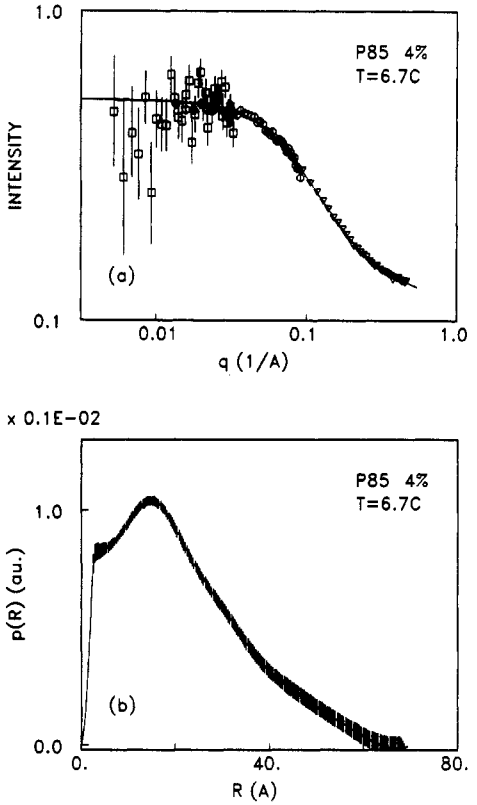

Figure 2. (a) Scattering function of 4 wt % $EO_{25}PO_{40}EO_{25}$ dissolved in D_2O, as obtained at 6 °C using three instrumental settings (see text). (b) The corresponding pair-correlation function obtained by Fourier transformation. The scattering function reveals independent Gaussian polymer chains with R_g = 17 Å.

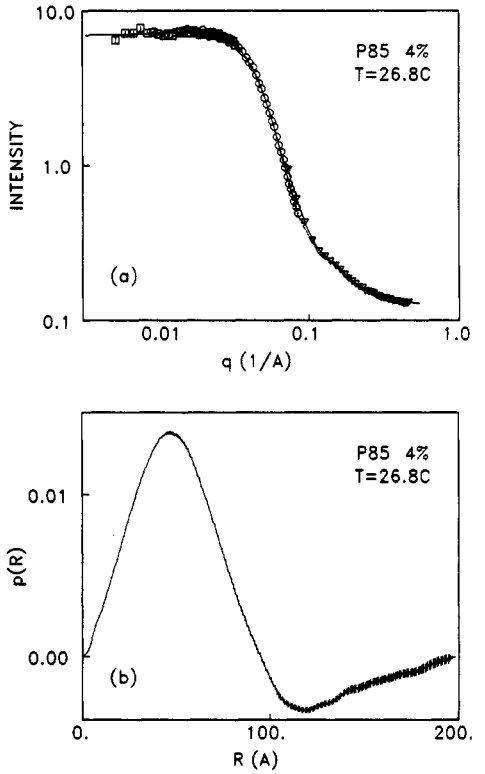

Figure 3. (a) Scattering function of 4 wt % $EO_{25}PO_{40}EO_{25}$ dissolved in D_2O, as obtained at 26 °C using three instrumental settings (see text). (b) The corresponding pair-correlation function obtained by Fourier transformation. The scattering pattern reveals the spherical micelle.

the degree of polymerization of both propylene oxide (n) and ethylene oxide (m).[15] For a range of materials to which

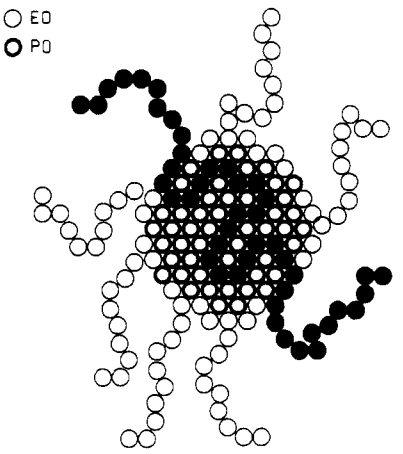

Figure 4. Schematic model of the PEO–PPO–PEO spherical micelle. The effective core consists of PO and a dense monolayer shell of EO. The black-colored monomers show schematically the imagined form of a single PEO–PPO–PEO chain. The chain conformation could also be U-shaped.

$EO_{25}PO_{40}EO_{25}$ belongs, the aggregates are in the form of micelles;[5] i.e., the aggregates are in the form of a core presumably dominated by propylene oxide blocks and surrounded by a corona of hydrated ethylene oxide subchains.

In a given temperature range, the micelles are in thermodynamic equilibrium with the unimers

$$\text{unimers} \rightleftharpoons \text{micelles} \qquad (2)$$

with the equilibrium constants having a simple temperature dependence, as we show below. Figure 3a shows the scattering function as obtained at 26.8 °C for a 4 wt % polymer solution. Although both micellar aggregates and unimers are present in the solution at this temperature, the measured scattering function is dominated by the large aggregates, because the scattering function of an object is proportional to the squared volume. Figure 3b shows the corresponding pair-correlation function calculated from the scattering function of Figure 3a. The $p(R)$ function is dominantly bell-formed, suggesting that the aggregates consist of spherical micelles, relatively monodisperse in size with a radius $R_c \sim 50$ Å. A small negative minimum in $p(R)$ indicates that concentration effects to a small extent influence the scattering function at this temperature. As will be discussed below, this intermicellar correlation becomes the dominating component in the scattering function at higher temperatures. The radius resulting from the $p(R)$ calculation is presumably the size of the core of the micelles, as the outer corona of PEO chains has a much lower density. The radius is in good agreement with the value obtained at similar temperatures for higher concentrations, as discussed below (see also Figure 6). In comparison, the hydrodynamic radius, as obtained using dynamic light scattering,[5] is R_h = 80 Å, in agreement with the expectation that the hydrodynamic radius to a large extent also includes the corona.

The scattering pattern of disclike micelles, or very elongated ellipsoidal or rodlike micelles, would deviate significantly from the form shown in Figure 3, and also significant polydispersity would show up in the pair-correlation function, $p(R)$, as a long tail at high R values. We therefore conclude that the micelles, on average, approach a spherical form.

The observed scattering function, on the other hand, does not show the characteristic ripples and the q^{-4} approach at large q values as expected for a monodisperse suspension of spheres with a sharp interface, having the

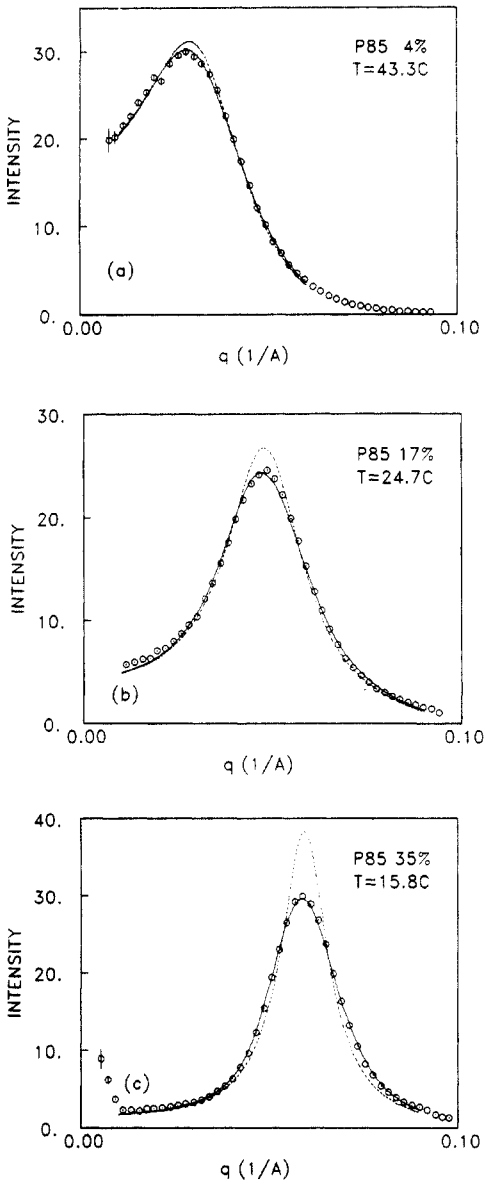

Figure 5. Typical examples of the scattering function of EO_{25}-$PO_{40}EO_{25}$ dissolved in D_2O, revealing a highly correlated micellar liquid. The three data sets represent polymer concentrations of 4 (a), 17 (b), and 35 wt % (c), as obtained at 43.3, 24.7, and 15.8 °C, respectively. The solid lines are the best fits using the hard-sphere Percus–Yevick approach and including instrumental smearing. The dotted lines represent the same scattering curves with no instrumental smearing.

form factor

$$P(q) = \left[\frac{3}{(qR_c)^3}(\sin(qR_c) - qR_c\cos(qR_c))\right]^2\left(\frac{4\pi}{3}R_c\right)^2 \quad (3)$$

characterized by the sphere radius R_c. These deviations are attributed to the ethylene oxide subchains dispersed in the water phase, in agreement with a simplified model of the micellar structure with a central, dense core of dominantly poly(propylene oxide) and an outer corona of hydrated poly(ethylene oxide) effectively grafted onto the surface of the core, as schematically illustrated in Figure 4.

As the temperature, or the concentration, is increased, the scattering function becomes dominated by a pronounced correlation peak revealing significant micelle–micelle interaction (cf. Figure 5). Correspondingly, the pair-correlation function exhibits a marked negative minimum (curve *a* in Figure 11). Within the q range well beyond the correlation peak, on the other hand, the scattering function remains effectively unchanged, indicating that the changes in the observed scattering function first of all reflect an increasing density of micelles, whereas the characteristics of the individual micelles are relatively unaffected by increasing temperature or concentration.

C. Micelle Correlation. While the scattering function of dilute suspensions, where no interference occurs between scattering from different particles, is given by the form factor $P(q)$, interference becomes significant in more dense suspensions. For a monodisperse system of particles, the scattering function can be written as a product of the single-particle form factor and a structure factor, $S(q)$, describing the interparticle interference:

$$I(q) = \Delta\rho^2 N P(q)\, S(q) \quad (4)$$

where $\Delta\rho^2$ is the contrast factor and N is the number density of scatterers. Although it is clear from the low temperature, low polymer concentration study discussed below that the micelles do not have a sharp surface, we will as a first approach analyze the data in terms of dense spheres, using the form factor according to eq 3. The structure factor is given by[16]

$$S(q) = 1 + 4\pi N\int (g(R) - 1)\frac{\sin(qR)}{qR}R^2\, dR \quad (5)$$

where $g(R)$ is the radial distribution function describing the arrangement of the micelles. In the Ornstein–Zernike approximation the correlation fluctuations

$$h(R) = g(R) - 1 \quad (6)$$

are written as the sum of a direct, short-range correlation between any two micelles (1 and 2 distanced $R = R_{12}$), $f(R_{12})$, and an indirect term by which the correlation is transferred to all of the neighboring particles

$$h(R_{12}) = f(R_{12}) + N\int f(R_{13})\, g(R_{32})\, dR_3 \quad (7)$$

Now using the Percus–Yevick expression for the short-range term[17]

$$f(R) = (e^{\Phi(R)/kT} - 1)e^{\Phi(R)/kT}g(R) \quad (8)$$

with $\Phi(R)$ describing the steric interactions between neighboring micelles, as given by a hard-sphere interaction potential

$$\Phi(R) = \infty \quad \text{for } R < R_{hs}$$

$$\Phi(R) = 0 \quad \text{for } R \geq R_{hs} \quad (9)$$

characterized by the hard-sphere interaction radius R_{hs}. The hard-sphere model is not unique in being able to fit the data. Other interaction potentials could probably also fit the experimental data, but generally these would need more parameters, and thereby more information is extracted from the data than these really give the basis for. The hard-sphere interaction gives, moreover, a very simple interpretation of the data. Equation 7 leads to a polynomial solution for $f(R)$

$$f(R) = -(\alpha + \beta r + \gamma r^3) \quad (10)$$

where α, β, and γ are given by the hard-sphere volume fraction ϕ

$$\alpha = (1 + 2\phi)^2/(1 - \phi)^4$$

$$\beta = -6\phi(1 + \phi/2)^2/(1 - \phi)^4$$

$$\gamma = (\phi/2)(1 + 2\phi)^2/(1 - \phi)^4$$

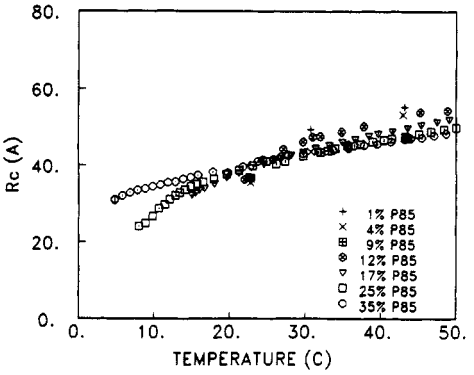

Figure 6. Resulting core radius, R_c, as obtained by fitting the hard-sphere Percus–Yevick model to the scattering data.

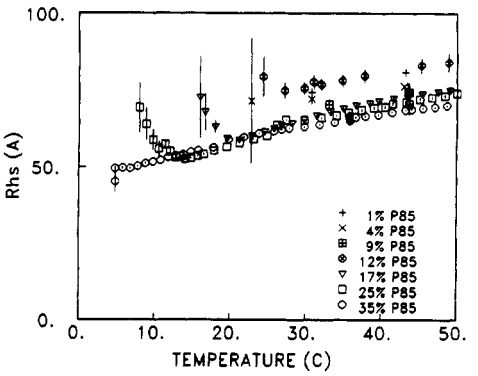

Figure 7. Resulting hard-sphere interaction-radius, R_{hs}, as obtained by fitting the hard-sphere Percus–Yevick model to the scattering data.

and r is the reduced distance

$$r = R/2R_{hs}$$

Incorporating these approaches leads to an analytical result for the structure factor[18,19]

$$S(q) = \frac{1}{1 + 24\phi G(2qR_{hs},\phi)/(2qR_{hs})} \tag{11}$$

where G is a trigonometric function of $x = 2qR_{hs}$ and ϕ

$$G(x,\phi) = (\alpha(\phi)/x^2)[\sin(x) - x\cos(x)] + (\beta(\phi)/x^3) \times [2x\sin(x) + (2 - x^2)\cos(x) - 2] + (\gamma(\phi)/x^5) \times [-x^4\cos(x) + 4[(2x^2 - 6)\cos(x) + (x^3 - 6x)\sin(x) + 6]] \tag{12}$$

Thus, the scattering function is in an analytical form determined by the hard-sphere volume fraction ϕ and the two radii characteristic for the micelles: the core radius R_c and the hard-sphere interaction radius R_{hs}. The analytical formula for the scattering function can easily be incorporated in a least-squares fitting routine, which also includes smearing due to instrumental resolution as obtained in a Gaussian approximation.[11]

Excellent fits are obtained to the experimental scattering function for q values up to approximately 2–3 times the peak position q_0. This is shown in typical examples given in Figure 5. The solid lines in Figure 5 give the fitted scattering functions including smearing according to the instrumental setup. The dotted lines represent the same scattering functions with no smearing. For q values beyond the order of $3q_0$ significant deviation from the hard-sphere approximation is observed. While the analytical approach used for large q values gives an approximate q^{-4} dependence due to the spherical form factor, eq 3, the experimental data give rather an $I \sim q^{-2.6}$ relationship, reflecting the soft corona given by the hydrated PEO chains dispersed in the water. In the fittings presented below, we have restricted the q range to 0.01–0.08 Å, which results in fits with a mean square residual, χ^2, typically of the order of 2–5.

From the fits we obtained information on micellar core radius, hard-sphere interaction radius, and micellar (hard sphere) volume fraction as a function of temperature and polymer concentration. Very simple relationships appear from these results, as shown in Figures 6–8. The micellar core radius (R_c) and hard-sphere radius (R_{hs}) appear to be basically independent of polymer concentration, as seen from the resulting parameters displayed in Figures 6 and 7. A distinct increase in both R_c and R_{hs} at increaisng temperatures probably reflects changes in aggregation number but can also be attributed to conformational changes or changes in hydration of the polymer chains.

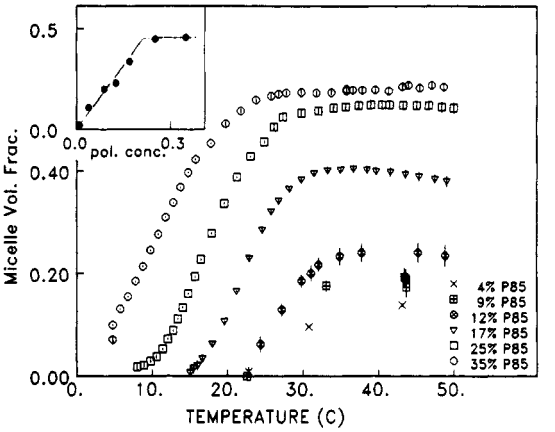

Figure 8. Resulting hard-sphere volume fraction, ϕ, as obtained by fitting the hard-sphere Percus–Yevick model to the scattering data. The insert shows the 30 °C value of the limiting volume fraction ϕ_0 versus polymer concentration.

The core radius changes from approximately 30 Å at 5 °C to 50 Å at 50 °C. Simultaneously, the hard-sphere interaction radius changes from 50 to 70 Å; i.e., the micelles have a ~20-Å PEO shell. The hard-potential character of this shell must reflect steric interactions between polymers, but in addition one can speculate at the role of structured water within the micelle shell.

Most important for the phase behavior of the polymer solution are, however, the changes in hard-sphere volume fraction, ϕ, as a function of temperature and polymer concentration. In Figure 8 is shown the resulting volume fraction as a function of temperature for various polymer concentrations in the 4–35 wt % range. Above a critical micellation temperature (T_{cm1}) and a critical micellation concentration (c_{cm}), the volume fraction appears roughly linear in both temperature and polymer concentration until a saturated value, ϕ_0, is reached at T_{cm2}.

In the insert of Figure 8 is shown the concentration dependence of the saturation limit ϕ_0. For polymer concentrations below approximately 20 wt %, the saturation limit, ϕ_0, varies linearly with concentration, in agreement with expectations for ϕ_0 corresponding to the situation that all polymers have aggregated in micelles. Above $c \sim 20$ wt %, on the other hand, the micelle volume fraction remains constant at $\phi_c \sim 0.53$. This is the maximum possible volume fraction, being the critical value for hard-sphere crystal formation.[8,20] In Figures 6–8 we also include fits made to data obtained within the crystalline phase, although the Percus–Yevick analysis is valid only for liquids. However, because the bond correlation remains basically liquid-like within the crystalline phase,[6,8] the Percus–Yevick analysis still gives good fits.

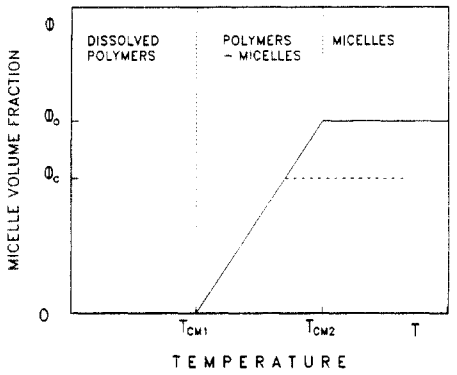

Figure 9. Schematic representation of the temperature-dependent micellar volume fraction. For $T < T_{cm1}$, PEO–PPO–PEO chains are dissolved as independent Gaussian chains. In the $T_{cm1} < T < T_{cm2}$ regime, independent polymer chains exist in equilibrium with micelles. For $T_{cm2} < T$, all polymers have aggregated into micelles. The dotted curve represents the situation that the critical value for hard-sphere crystallization (ϕ_c) is smaller than the value ϕ_0 corresponding to all polymers aggregated into micelles.

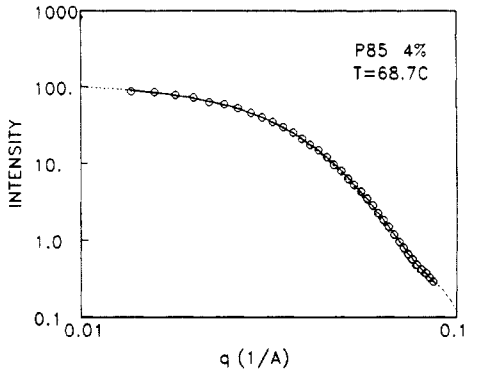

Figure 10. Scattering function of 4 wt % $EO_{25}PO_{40}EO_{25}$ dissolved in D_2O, as obtained at 68.7 °C.

The crystalline order might, though, have introduced some systematic errors in the results.

The relationships between micelle volume fraction and respectively temperature and polymer concentration can be written

$$\phi(T) \simeq \phi_0(T - T_{cm1}) \quad \text{for } T_{cm1} < T < T_{cm2} \text{ and } \phi < \min(\phi_c, \phi_0)$$

$$\phi(c) \simeq \phi_0(c - c_{cm}) \quad \text{for } T_{cm1} < T \text{ and } \phi < \phi_c \qquad (13)$$

In Figure 9, these equations are shown schematically, neglecting the temperature-dependent changes in micellar sizes, which are responsible for the small decrease in micelle concentration observed experimentally (Figure 8). A linear relationship appears between the critical micellation temperature (T_{cm1}) and the critical micellation concentration (c_{cm})

$$T_{cm1}(c) = T^{\circ}_{cm1}(1 - c_{cm}/c_{cm}(0)) \qquad (14)$$

with T°_{cm1} = 32 °C being the value for polymer concentration approaching zero. $c_{cm}(0) \sim 36$ wt % is the critical polymer concentration at 0 °C. Equation 14 is represented by the $\phi = 0$ line in the phase diagram (Figure 13) shown below.

In the regime where ϕ increases linearly with temperature, the system is thermodynamically stable with both micelles and polymers present (eq 2). The number of micelles per volume, ϕ/V_m ($V_m = 4\pi/3R^3_{hs}$ being the hard-sphere micelle volume), and the number of free chains per volume, n_p, are related through

$$n_p + N\phi/V_m = c/V_p \qquad (15)$$

where V_p is the dry volume of the polymer and N is the aggregation number. Assuming that the saturation in volume fraction, ϕ_0, corresponds to no free polymer chains, i.e., $n_p = 0$ for $\phi = \phi_0$, thereby leads to the aggregation number:

$$N = (c/\phi_0)(4\pi R^3_{hs}/3V_p) \qquad (16)$$

The dry polymer volume is given as the sum of the volume of monomers, $V_p = 2mV_{EO} + nV_{PO}$, where

$$V_i = M_i/(\rho_i N_A) \quad i = \text{PO or EO} \qquad (17)$$

With the molar weight $M_{PO} = 58$ and the mass density $\rho_{PO} = 1.01$ g/cm^3 the propylene oxide volume is $V_{PO} = 95.4$ Å^3, and with $M_{EO} = 44$ and $\rho_{EO} = 1.01$ g/cm^3 the ethylene oxide volume is $V_{EO} = 72.4$ Å^3. Using the value for R_{hs} as shown in Figure 7, we then get an aggregation number of $N \sim 37$ at 20 °C, increasing to 78 at 40 °C.

The aggregation number can independently be obtained from the knowledge of the core dimension. If we assume that the core consists only of propylene oxide, we have

$$4\pi R^3_c/3 = NnV_{PO} \qquad (18)$$

where $n = 40$ is the poly(propylene oxide) degree of polymerization. This leads to an aggregation number of $N \sim 58$ to $N \sim 116$ in the same temperature range. If we, on the other hand, use a more realistic model where the core dimensions, as obtained from the hard-sphere model, are given by a dense propylene oxide core covered by a dense monolayer shell of ethylene oxide (see Figure 4), we get, within the whole temperature regime, perfect agreement between the two routes of calculating the aggregation number. The resulting thickness of the dense EO shell is 2.8 Å.

The changes in the micellar sizes with temperature show that the micelles are dynamic aggregates in which the individual polymer chains constantly move from one micelle to another. This allows optimizing the aggregation number according to temperature-dependent thermodynamic parameters. The micelle illustrated in Figure 4 should accordingly be viewed as an idealized picture of a snapshot of the aggregate.

D. High-Temperature Properties. At temperatures above approximately 70 °C the scattering function changes pronouncedly in character. In the low-concentration regime, the characteristic correlation peak totally disappears, as seen in Figure 1a and in Figure 10, showing the scattering data of the 4 wt % sample as obtained at T = 68.7 °C. In the higher concentration regime, the form of the correlation peak changes, with significant increase in the low-q intensity (Figure 1b,c). For polymer concentrations above 20 wt %, in which the cubic phase is observed, the crystalline phase melts within the same temperature range.[8]

Figure 11 shows the pair-correlation function, $p(R)$, of the 4 wt % polymer concentration, corresponding to the T = 68.7 °C scattering function shown in Figure 10, as well as $p(R)$ calculated from data obtained both within the correlated regime (T = 51.7 °C) and at higher temperatures (T = 77.5 °C and T = 86.1 °C). The 51.7 °C $p(R)$ function shows a pronounced negative regime reflecting the highly correlated micelles with excluded volume due to hard-sphere repulsion. The high-temperature aggregates show distinct differences from the low-temperature micelles. As the temperature is increased beyond approximately 70

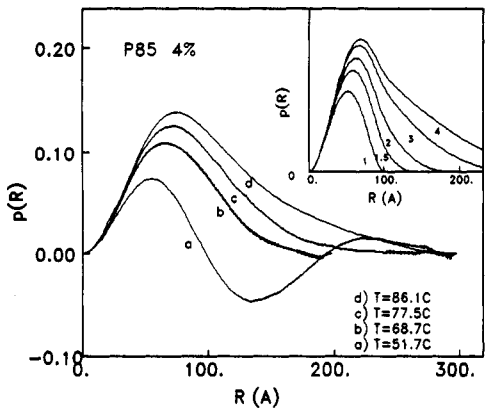

Figure 11. Pair-correlation function of 4 wt % $EO_{25}PO_{40}EO_{25}$ dissolved in D_2O, as obtained from Fourier transformation of scattering functions obtained at 51.7, 68.7, 77.5, and 86.1 °C. The insert shows calculated $p(R)$ functions for a sphere (1) and for prolate ellipsoids with axis ratios 1:1:1.5, 1:1:2, 1:1:3, and 1:1:4, as identified by the values 1.5, 2, 3, and 4, respectively, in the figure.

°C, the aggregates become still more dispersed, with tails in the pair-correlation function up to more than 250 Å. This should be compared with the well-defined spherical micelles with maximum distances of 100 Å close to ambient temperatures (Figure 3b). The $p(R)$ function thus indicates structural changes in the micelles, from globular aggregates to larger prolate ellipsoids. For comparison, numerical calculations of $p(R)$ functions for prolate ellipsoids with axis ratios 1:1:1 (sphere), 1:1:1.5, 1:1:2, 1:1:3, and 1:1:4 are shown in the insert of Figure 11. The $p(R)$ curves were calculated corresponding to fixed volume fraction and subsequently normalized by the micellar volume. While these $p(R)$ functions show striking similarity with the experimental data, oblate ellipsoids result in quite different curves.[21]

For the high-concentration samples the structure factor still dominates the scattering function, and detailed information on the form of the aggregates cannot be gained from the present data. The observed scattering function is very similar to that seen in the L_3 phase of low molecular weight surfactants, in which a three-dimensional continuous disordered bilayer structure is formed.[22] One could therefore speculate in the formation of a microemulsion at high concentrations. It is, however, more likely that also the high-concentration micelles develop into an ellipsoidal form, which further develops into long rods. At even higher temperature, these rods undergo a disorder-to-order transition, forming a hexagonal structure, as shown by shear experiments.[8]

The origin of the changes in micelle structure close to $T = 70$ °C may be related to the size of the spherical aggregates just below this temperature. As seen from the hard-sphere Percus–Yevick analysis, the core radius increases with increasing temperature (Figure 6). Close to $T = 70$ °C, the core radius of approximately 50 Å gives on average only 2.5 Å per PO monomer for those chains crossing the micelle center; i.e., these linear PPO blocks must be stretched to the maximum. It is therefore, first of all, not possible to increase the size of a spherical micelle further. Moreover, this conformation is entropically very unfavorable and may very well be the driving force for the changes in micelle structure from spherical form to prolate ellipsoid. Another driving force for the high-temperature changes could be changes in the hydration level of PEO. Other PEO-containing amphiphilic molecules, e.g., C_nEO_m systems,[23] show marked structural changes in the same temperature range.

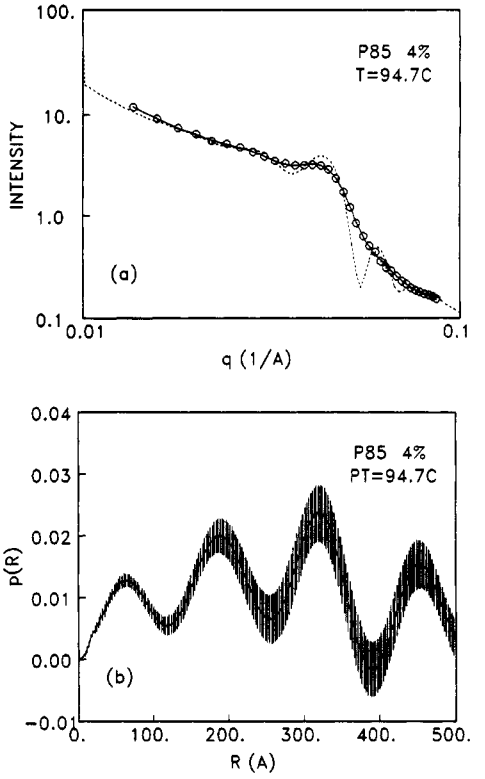

Figure 12. Scattering function of 4 wt % $EO_{25}PO_{40}EO_{25}$ dissolved in D_2O, as obtained at 94.7 °C (a) and the corresponding pair-correlation function obtained by Fourier transformation (b). The full line in (a) is the fit including instrumental smearing. The dotted line represents the corresponding scattering function with no smearing.

At the highest temperature studied, close to 100 °C, further changes appear in the aggregate structure, as seen in the neutron scattering data shown in Figure 12a, but also in light scattering, as the suspension changes from transparent to opaque, indicating formation of large, micrometer-sized aggregates. These changes are most probably related to ethylene oxide, which is known to undergo a transition to a fully dehydrated state in this temperature regime.[24] The high-temperature neutron scattering data show characteristics quite different from the low-temperature pattern. The Fourier-transformed $p(R)$ function (Figure 12b) shows regular oscillations, indicating an ordered structure. Actually, the scattering profiles are, to a great extent, similar to theoretical calculations of the scattering function of very swollen lamellae phases, taking concentration fluctuations with local displacements within the layers into account.[25]

IV. Conclusions

In conclusion, we have by structural studies obtained detailed information on the phase behavior of the P85 poloxamer $EO_{25}PO_{40}EO_{25}$. In Figure 13, we summarize the resulting phase diagram, including the crystalline cubic and hexagonal phases presented before.[8] In the low temperature, low polymer concentration corner, the polymers are fully dissolved, independent Gaussian coils. Above the phase line of critical micellation, polymers and micelles are in thermodynamic equilibrium. Above a second phase line, all polymers have aggregated into micelles. The intermicellar correlations can, to a very good approximation, be described in terms of hard-sphere interactions. As the micellar (hard sphere) volume fraction approaches 0.53, the micelles crystallize in a cubic lattice, as shown before.[6,8] The micelles are spherical with a core of propylene oxide surrounded by a dense monolayer of ethylene oxide and

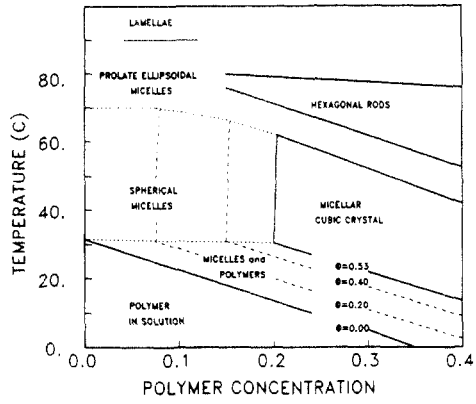

Figure 13. Temperature–concentration phase diagram showing the characteristics of $EO_{25}PO_{40}EO_{25}$ fully dissolved in D_2O. In the low-concentration, low-temperature range, the polymers are dissolved Gaussian chains. Above the $\phi = 0$ line of critical micellation concentration/temperature, a liquid of micelles is formed with micellar volume fraction (ϕ) as shown by contour lines in the figure. When the $\phi = 0.53$ line is crossed, the micellar liquid "freezes" into a hard-sphere cubic crystal.[8]

an outer corona of flexible poly(ethylene oxide) blocks. The micellar size, and thereby the aggregation number, increases with temperature. The micelles must be viewed as rather dynamic aggregates in which the PEO–PPO–PEO chains constantly move from micelle to micelle. This allows optimizing the micellar size according to thermodynamic parameters. Close to $T = 70$ °C, the diameter of the micellar core becomes of the order of magnitude of the fully stretched PPO block. This may be the driving force for dramatic changes in the aggregate conformation, transforming the spherical micelles into prolate ellipsoids. At even higher temperatures, a lamella phase appears.

Acknowledgment. We thank Wyn Brown (Uppsala University), Walter Batsberg (Risø National Laboratory), and Søren Hvidt (Roskilde University Center) for fruitful discussions. Financial support from the Danish Natural Science Research Council is gratefully acknowledged.

References and Notes

(1) Rassing, J.; Attwood, D. *Int. J. Pharm.* **1983**, *13*, 47–55.
(2) Zhou, Z.; Chu, B. *Macromolecules* **1987**, *20*, 3089–3091.
(3) Zhou, Z.; Chu, B. *J. Colloid Interface Sci.* **1988**, *126*, 171–180.
(4) Wanka, G.; Hoffmann, H.; Ulbricht, W. *Colloid Polym. Sci.* **1990**, *268*, 101–117.
(5) Brown, W.; Schillen, K.; Almgren, M.; Hvidt, S.; Bahadur, P. *J. Phys. Chem.* **1991**, *95*, 1850–1858.
(6) Mortensen, K.; Brown, W.; Nordén, B. *Phys. Rev. Lett.* **1992**, *13*, 2340–2343.
(7) Mortensen, K. *Colloid Polym. Sci.*, in press.
(8) Mortensen, K. *Europhys. Lett.* **1992**, *19*, 599–604.
(9) Vadnere, M.; Amidon, G. L.; Lindenbaum, S.; Haslam, J. L. *Int. J. Pharm.* **1984**, *22*, 207–218.
(10) Wang, P.; Johnston, T. P. *J. Appl. Polym. Sci.* **1991**, *43*, 283–291.
(11) Pedersen, J. S.; Posselt, D.; Mortensen, K. *J. Appl. Crystallogr.* **1990**, *23*, 321–333.
(12) Glatter, O. *J. Appl. Crystallogr.* **1977**, *10*, 415–521.
(13) Hansen, S.; Pedersen, J. S. *J. Appl. Crystallogr.* **1991**, *24*, 541–548.
(14) Svergun, D. I.; Pedersen, J. S., unpublished.
(15) Mortensen, K.; Brown, W., to be published.
(16) Guinier, A.; Fournet, G. *Small Angle Scattering of X-Rays*; Wiley: New York, 1955.
(17) Percus, J. K.; Yevick, G. J. *Phys. Rev.* **1958**, *110*, 1–13.
(18) Ashcroft, N. W.; Lekner, J. *Phys. Rev.* **1966**, *145*, 83–90.
(19) Kinning, D. J.; Thomas, E. L. *Macromolecules* **1984**, *17*, 1712–1718.
(20) Pusey, P. N.; van Megen, W. *Nature* **1986**, *320*, 340–342.
(21) Glatter, O. *J. Appl. Crystallogr.* **1979**, *12*, 166–175.
(22) Strey, R.; Schomäcker, R.; Roux, D.; Nallet, F.; Olsson, U. *J. Chem. Soc., Faraday Trans.* **1990**, *86*, 2253–2261.
(23) Mitchell, D. J.; Tiddy, G. J. T.; Waring, L.; Bostock, T.; McDonald, M. P. *J. Chem. Soc., Faraday Trans. 1* **1983**, *79*, 975–1000.
(24) Karlström, G. *J. Chem. Phys.* **1985**, *89*, 4962–4964.
(25) Porte, G.; Marignan, J.; Bassereau, P.; May, R. *Europhys. Lett.* 1988, *7*, 713–717.